Research Square

Preprints are preliminary reports that have not undergone peer review.
They should not be considered conclusive, used to inform clinical practice,
or referenced by the media as validated information.

Dynamical Reliability, Memory Retention and Information- Processing Capacity of a Six-Dimensional Series Memcapacitor System

I. O. AJAYI

ajayiiyanu16@gmail.com

Bamidele Olumilua University of Education, Science and Technology

Research Article

Keywords: memcapacitor, reservoir computing, Lyapunov exponents, information-processing capacity, numerical reliability, memory retention, nonlinear dynamics

Posted Date: November 16th, 2026

DOI: https://doi.org/10.21203/rs.3.rs-11413535/v1

License: This work is licensed under a Creative Commons Attribution 4.0 International License.
Read Full License

Additional Declarations: No competing interests reported.

DYNAMICAL RELIABILITY, MEMORY RETENTION AND INFORMATION-PROCESSING CAPACITY OF A SIX-DIMENSIONAL SERIES MEMCAPACITOR SYSTEM

By

I. O. AJAYI

Department of Physics, Bamidele Olumilua University of Education, Science and Technology, Ikere Ekiti, Ekiti State.

Email: ajayiiyanu16@gmail.com, ajayi.iyanuoluwa@bouesti.edu.ng

Phone No.: 07031463948

ORCID NO.: 0009-0008-6399-0167

Abstract

This research examines whether the six-dimensional series-connected memcapacitor system can serve as a numerically reliable, input-driven computational substrate, and how its computational performance relates to the retention of its dynamical regime. A scalar input was added to the first state equation and the system was evaluated at six values of one coefficient, four coupling strengths, ten parameter, initial-state and solver scenarios per regime and five independent input realisations, giving 384 simulations. Lyapunov spectra were computed autonomously and along the driven trajectory, and memory, nonlinear and prediction performance were measured with ridge-regression readouts, a surrogate-based capacity threshold and reference predictors. At the published coefficients the leading exponent is $\lambda_1 = 0.080 \pm 0.011$ (two standard errors) and the second exponent is indistinguishable from zero, so the regime is chaotic with a single positive exponent. This classification was retained in 9 of 10 and 8 of 10 perturbation scenarios in the two chaotic regimes and was lost only under ±5% perturbations, while the driven chaotic system escaped to infinity in four of five input realisations at the strongest coupling. Chaotic trajectories separated after 134 to 357 time units, whereas the Lyapunov estimates were insensitive to step size. Linear memory capacity reached 2.6 in non-chaotic regimes and was zero in the chaotic regimes and in a marginal non-chaotic regime. Nonlinear capacity was not found in the dynamics, and three of the six coordinates carried the useful information. NARMA-10 prediction ($R^2 = 0.47$ to 0.49) exceeded the mean but not a linear delay-line reference (0.66). Dynamical reliability and computational usefulness are therefore related but distinct. The results provide a quantitative framework for assessing memcapacitive systems as reservoirs, within the limits of a noiseless numerical model.

Keywords: memcapacitor; reservoir computing; Lyapunov exponents; information-processing capacity; numerical reliability; memory retention; nonlinear dynamics.

INTRODUCTION

Memcapacitors are memory-dependent electrical elements whose constitutive responses depend on their internal states and the history of applied electrical signals. When incorporated into nonlinear circuits, they introduce additional state-dependent interactions that can produce complex dynamical behaviour, including multistability, chaos and hyperchaos. These characteristics have attracted interest in nonlinear electronics because they provide opportunities to investigate both the evolution of memory-dependent systems and the possible use of their internal dynamics for information processing. The method for circuit elements with memory was first established by Di Ventra et al. (2009), providing a foundation for subsequent investigations of memcapacitive, memristive and meminductive systems. Later studies examined memcapacitor models, chaotic oscillators, coexisting attractors and other forms of nonlinear behaviour (Wang et al., 2016a, 2016b, 2017; Yuan et al., 2016, 2019). However, establishing that a memory-dependent circuit generates complex dynamics is different from demonstrating that its behaviour is reproducible under uncertainty or that its evolving states can perform useful computational tasks. The reliability of a nonlinear dynamical system concerns the extent to which its relevant properties remain reproducible under specified changes in parameters, initial conditions and numerical procedures. Conventional analyses of chaos commonly employ equilibrium calculations, bifurcation diagrams, Lyapunov exponents, phase portraits and basin-of-attraction visualisations. These methods are essential for characterising nonlinear behaviour, but their conclusions depend on the conditions under which the system is investigated. In a multistable system, different initial conditions can lead to different attractors, while changes in model parameters can alter the stability and accessibility of those attractors. Menck et al. (2013) introduced basin stability as a probabilistic measure of the likelihood that perturbations to initial conditions lead to a specified attractor. Brzeski et al. (2016) subsequently examined basin stability in multistable systems subject to parameter mismatch. These studies provide useful foundations for uncertainty-aware dynamical analysis. Nevertheless, a reliability assessment tailored to a particular nonlinear system must specify which properties are being retained, how uncertainty is introduced and how the resulting outcomes are classified.

Numerical fidelity is particularly important when reliability is assessed through computational experiments. Numerical integration approximates the evolution of the governing differential equations, while Lyapunov exponents and other dynamical indicators are estimated over finite observation intervals. Inadequate transient removal, insufficient measurement duration, inappropriate integration steps and incomplete convergence can influence the inferred dynamical regime. Skokos (2010) reviewed methods for computing Lyapunov characteristic exponents and discussed the numerical considerations involved in their estimation. For high-dimensional nonlinear systems, therefore, it is necessary to distinguish a genuine change in the underlying dynamics from an apparent transition arising from the numerical procedure. This requirement becomes even more important when dynamical simulations are subsequently used to evaluate a system's computational performance. If the state trajectories or classifications are not numerically trustworthy, conclusions about memory retention and information processing may also be unreliable. Numerical convergence should consequently be established as a prerequisite for computational assessment rather than treated as an optional supplementary test.

This change in research perspective is important because a dynamical model and a computational reservoir are not equivalent descriptions of a system. The published memcapacitor model is formulated as an autonomous nonlinear dynamical system, whereas reservoir computing requires a mechanism through which an external input influences the evolving state. In reservoir computing, the internal dynamics transform an input sequence into a state representation, from which a comparatively simple readout is trained to produce the required output (Lukoševičius & Jaeger, 2009). In physical reservoir computing, the evolving states of an electronic circuit or other physical substrate provide the computational resource. The effectiveness of such a reservoir depends on the relationship between input encoding, state evolution, memory retention, nonlinear processing and output measurement. Recent reviews have emphasised that the complexity of a physical substrate alone does not establish its computational usefulness; the input-driven architecture and task-specific performance must also be characterised (Liang et al., 2024; Tanaka et al., 2019; Stepney, 2024). The computational potential of a nonlinear dynamical system can be examined through the information-processing-capacity framework developed by Dambre et al. (2012). This framework quantifies how accurately a driven system can reproduce specified functions of its input history and distinguishes linear from nonlinear information-processing tasks. Such measurements are particularly relevant to memory-dependent circuits because they allow the computational properties of the evolving states to be assessed independently of the visual complexity of their trajectories. Inubushi and Yoshimura (2017) investigated the relationship between memory and nonlinear processing in reservoir computing, while Gauthier et al. (2021) developed a next-generation reservoir-computing framework based on nonlinear transformations of time-delayed inputs. These studies provide methodological foundations for investigating whether the internal states of a memcapacitive system retain useful information and transform that information into representations suitable for computation.

An important point is that chaos and hyperchaos should not be treated as direct measures of computational capacity. Strong sensitivity to initial conditions and complex state evolution may generate diverse dynamical responses, but they do not necessarily guarantee that a reservoir preserves relevant input information or produces representations that a trained readout can exploit. A system with substantial dynamical complexity may have limited useful memory for a particular input encoding, while a less irregular regime may provide better performance on a specified task. The relationship between memory retention and nonlinear processing must therefore be measured rather than assumed. Prediction performance provides an additional test of practical computational usefulness, but it is also task-dependent. A low prediction error on one benchmark does not, by itself, establish broad information-processing capacity or general computational superiority. A defensible evaluation should combine capacity measurements with a clearly defined prediction task, consistent training and testing procedures, and comparisons against appropriate reference models.

The nominal dimension of the memcapacitive system also requires careful consideration. Although the model contains six state coordinates, these coordinates cannot automatically be interpreted as six independent sources of computational information. Algebraic constraints, invariant relationships and correlations between state trajectories may reduce the effective information available to a readout. The published equations and their invariant properties must therefore be examined before

the computational state vector is selected. Where justified, alternative representations of the state variables can be compared to determine whether particular coordinates contribute useful information beyond that already represented by the remaining states. This analysis is important for distinguishing nominal state dimension from effective computational dimension and for determining whether a reduced state representation can retain the relevant information while simplifying the readout. It also provides a direct connection between the mathematical structure established in previous dynamical studies and the new computational investigation. The relationship between dynamical reliability and computational performance introduces a further issue. A system may retain its broad dynamical classification under parameter perturbations while its memory capacity or prediction performance changes substantially. Conversely, a change in dynamical classification need not automatically imply a loss of computational usefulness. The two properties must therefore be assessed independently before their relationship can be established. For a memcapacitive system considered as a potential computational substrate, the relevant issue is not simply whether a chaotic regime exists, but whether useful computational performance can be demonstrated under operating conditions whose numerical behaviour has been adequately validated. Investigating this relationship requires matched experiments in which dynamical reliability, information-processing capacity and prediction performance are evaluated under comparable parameter conditions.

The published studies of Adelakun et al. (2026) and Ajayi (2026) established the model-specific foundations for this research: the former reported the hyperchaotic dynamics, multistability and circuit realisation of the six-dimensional series-connected memcapacitor system, and the latter characterised its chaotic dynamics, equilibrium manifold, dissipativity, boundedness and invariant memory relation. What remains unresolved is a problem that neither study was designed to address. It is not known whether the dynamical regime of the system is reproducible under controlled numerical and parameter uncertainty, whether the system retains and transforms the history of an external input in a way that a trained readout can exploit, how many of its six nominal coordinates contribute independent computational information, or whether reproducible dynamics and useful computation coincide. Without a unified quantitative assessment that links these properties under matched operating conditions, the computational potential of the system can only be asserted from the visual complexity of its trajectories. This is a targeted research gap and not a claim that uncertainty quantification or reservoir computing is absent from the wider literature; the extent to which closely related studies have already addressed exactly this combination would require a systematic review before the gap is claimed as globally unprecedented.

Motivated by these observations, the present research treats the established system as a candidate input-driven reservoir. Instead of introducing another model or repeating the established attractor and basin analyses, it performs a controlled computational investigation in which the system is driven by an external input and its dynamical reliability and computational performance are measured on the same simulated conditions. All numerical simulations are implemented in Python. The aim of this research is to develop and apply an uncertainty-aware computational framework that evaluates the linear memory, nonlinear information-processing capacity and prediction performance of the six-dimensional series-connected memcapacitor system, and determines how these computational properties relate to the numerical reliability and dynamical-regime retention of the system under controlled operating

conditions. Specifically, this study seeks to (i) establish the numerical convergence of the selected operating conditions and quantify the retention of a pre-defined dynamical classification under controlled parameter and initial-state perturbations; (ii) formulate the system as an explicitly input-driven reservoir by specifying the input-coupling mechanism, the observable state vector and the readout architecture; (iii) quantify the linear memory capacity and the nonlinear information-processing capacity using established reservoir-computing measures; (iv) examine the computational contribution of the observable state variables by comparing mathematically justified alternative state representations; (v) evaluate out-of-sample prediction performance with consistent training, validation and testing procedures and appropriate reference models; and (vi) determine how dynamical-regime retention, numerical robustness, information-processing capacity and prediction performance vary across matched operating conditions, identifying the circumstances in which reliable dynamics coincide with useful computational performance and those in which they do not.

The main contribution of this work therefore lies not in proposing a new nonlinear model but in the evidence-based connection between the numerical reliability of the dynamics of a memcapacitive system and its demonstrated computational capacity. By distinguishing the existence of complex dynamics from measured computational capacity, the study identifies the conditions under which the six-dimensional memcapacitor system provides a useful representation of input history and the circumstances in which its computational performance is limited. The conclusions are restricted to the numerical model and the input-driven architecture specified in this study; claims about a physical reservoir would require corresponding circuit-level validation.

METHODOLOGY

Mathematical Model

This research is based on the six-dimensional series-connected memcapacitor system proposed by Adelakun et al. (2026) and analysed dynamically by Ajayi (2026). The system consists of two series-connected nonlinear memcapacitive elements coupled through an active nonlinear feedback network. The model equations are used without modification. The state vector is

$$\mathbf{X}(t)=[x(t), y(t), z(t), w(t), v_1(t), v_2(t)]^T, \tag{1}$$

where x, y, z and w denote the electrical state variables of the active nonlinear circuit, and v_1 and v_2 represent the internal memory-state variables of the two memcapacitive elements. The governing equations are

$$\dot{x}=az+bzw-x, \tag{2}$$

$$\dot{y}=dy+e_1yv_1^2+e_2yv_2^4-fz-gzw, \tag{3}$$

$$\dot{z}=\mathrm{h}y+j_1yv_1^2+j_2yv_2^4-kx, \tag{4}$$

$$\dot{w}=n_1z, \tag{5}$$

$$\dot{v}_1=y, \tag{6}$$

$$\dot{v}_2 = y, \tag{7}$$

where a,b,d,e_1,e_2,f,g,h,j_1,j_2,k and n_1 are constant parameters controlling the linear and nonlinear coupling among the state variables. The nominal parameter set and initial condition of the published study were adopted as the reference configuration.

Invariant Structure and Redundancy of the State

Equations (6) and (7) give $d(v_1 - v_2)/dt = 0$, so that

$$v_1(t) - v_2(t) = v_1(0) - v_2(0). \tag{8}$$

Because $v_1(0) = v_2(0)$ in the reference configuration, v_2 duplicates v_1 and the six coordinates reduce to five independent observables, x,y,z,w,v_1. The invariant is used as an integration check and as the basis for the choice of the observable state vector. Because equation (8) holds for any initial offset, it was also verified for $v_1(0) - v_2(0) = 0.1$.

Reservoir computing requires an explicit mechanism through which an external input influences the evolving state, whereas the published model is autonomous. A scalar input $u(t)$ was therefore added to the first state equation,

$$\frac{d\mathbf{X}}{dt} = \mathbf{F}(\mathbf{X};\boldsymbol{\theta}) + \kappa\, \mathbf{b}\, u(t), \qquad \mathbf{b} = [1,0,0,0,0,0]^T, \tag{9}$$

where $\mathbf{F}$ denotes the right-hand sides of equations (2) to (7), $\boldsymbol{\theta}$ is the parameter vector and κ is the coupling strength. Injection into x was adopted because the input vector has equal (zero) components for v_1 and v_2, so that the invariant (8) is preserved exactly; because the x-equation is the only one with a linear dissipative term; and because in preliminary exploratory runs on a separate random seed (seed 777), injection into y, z or w produced finite-time escape at $\kappa \geq 0.2$ whereas injection into x did not at weak coupling. The input is applied as a zero-order hold: sample u_i is constant on $[t_i, t_{i+1}]$ with $t_i = 0.1\, i$. Four coupling strengths, $\kappa \in \{0.01, 0.05, 0.10, 0.20\}$, were used, and a supplementary extension to $\kappa \in \{0.5, 1, 2, 4\}$ was run for the non-chaotic regimes. At the published coefficients the autonomous system is chaotic, and a chaotic substrate is not expected to have fading memory. To compare qualitatively different dynamics, the coefficient d was varied over $\{-0.4, -0.2, 0.0, 0.2, 0.35, 0.46\}$ with all other parameters and the initial condition unchanged; $d = 0.46$ is the published value. These values were fixed from the exploratory runs and span the non-chaotic to chaotic range. The input is an independent and identically distributed sequence uniform on $[-1,1]$, the standard excitation for information-processing-capacity measurements (Dambre et al., 2012), generated from a recorded root seed (20261016). Each reservoir experiment used $N = 6000$ samples (600 time units), the conditional Lyapunov calculations used 15,000 samples, and five independent input realisations (seeds 0 to 4) were used for the nominal parameters, with seed 0 used for the perturbation scenarios.

Numerical Integration and Convergence Verification

Driven trajectories were integrated interval by interval with the Dormand-Prince explicit Runge-Kutta method of order 8(5,3) (DOP853; Dormand & Prince, 1980; Hairer et al., 1993) in SciPy (Virtanen et al., 2020), with relative tolerance 10^{-10}, absolute tolerance 10^{-12} and maximum step 0.02, recorded on the 0.1 sampling grid.

Every trajectory was checked for finiteness with $\max|X|<10^{3}$ (otherwise it was labelled unbounded), for the expected length, and for the invariant error

$$E_{inv}=\max_i\left|\left(v_{1,i}-v_{2,i}\right)-\left(v_{1,0}-v_{2,0}\right)\right|\le 10^{-8}. \qquad (10)$$

Numerical convergence was assessed in three ways. Short-horizon agreement was tested by comparing the nominal driven trajectory with a $10^{-12}/10^{-14}$ DOP853 reference and with fixed-step fourth-order Runge-Kutta (RK4) at h=0.02, 0.01 and 0.005. The divergence horizon was measured by recomputing each nominal trajectory with a looser tolerance ($10^{-8}/10^{-10}$), a tighter tolerance ($10^{-12}/10^{-14}$) and an initial state perturbed by a relative 10^{-8} in all components (a replica), and defining t_{div} as the first time at which $\|\Delta\mathbf{X}\|_2>10^{-2}$; in a chaotic system a finite t_{div} is expected and is not an integration failure, and what is required is that statistical and classification quantities do not depend on it. Finally, the convergence of the Lyapunov estimates with integration time and with step size was examined.

Lyapunov Exponent Computation and Dynamical Classification

Lyapunov spectra were computed by the Benettin QR method (Benettin et al., 1980). The variational equation

$$\dot{\mathbf{Q}}=\mathbf{J}\left(\mathbf{X}(t)\right)\mathbf{Q}, \qquad \mathbf{Q}(0)=\mathbf{I}, \qquad (11)$$

where $\mathbf{J}=\partial\mathbf{F}/\partial\mathbf{X}$ is the Jacobian, was integrated together with the state by fixed-step RK4 (h=0.01), with QR re-orthonormalisation $\mathbf{Q}_{m+1}\mathbf{R}_m=\mathbf{\Phi}_m\mathbf{Q}_m$ every 0.1 time units, after a discarded transient of 200 time units (100 for the sweep over d). The exponents are

$$\lambda_i=\lim_{M\to\infty}\frac{1}{M\,\Delta\tau}\sum_{m=1}^{M}\ln\left|R_{m,ii}\right|, \qquad (12)$$

and were estimated as the mean of eight equal blocks of the retained record, with standard error

$$\mathrm{SE}_i=\frac{s_i}{\sqrt{8}}, \qquad (13)$$

where s_i is the standard deviation of the eight block estimates. Spectra were computed for the autonomous system (κ=0; 2,000 time units per scenario) and conditionally along the driven trajectory (1,500 time units). Because the input is additive it does not enter the Jacobian, so the conditional spectrum measures the sensitivity of the driven state to its initial condition.

Some exponents are zero by construction because of equation (8) and the equilibrium structure, so a zero band ε=0.01 was adopted, which is more than twenty times the largest scatter (0.0004) of structurally zero exponents at d=0. A trajectory is classified as hyperchaotic if $\lambda_2>\varepsilon$ and $\lambda_2>2\,\mathrm{SE}_2$, chaotic if $\lambda_1>\varepsilon$ and $\lambda_1>2\,\mathrm{SE}_1$ (and not hyperchaotic), and non-chaotic otherwise; diverging runs are unbounded. Class retention for a regime is the number of scenarios in Table 2 whose class equals that of the nominal scenario. The perturbation scenarios were the nominal case, simultaneous scaling of all twelve coefficients by $(1+\delta)$, scaling of all six initial-state components by $(1+\delta)$ with $\delta=\pm0.01,\pm0.05$, and a looser numerical setting (tolerance $10^{-8}/10^{-10}$ for

the driven runs and h=0.02 for the Lyapunov calculation), giving ten scenarios per regime and coupling.

The predictor for input u_i is the post-input observable state $\boldsymbol{\xi}_i=\mathbf{s}(t_{i+1})$ with

$$\mathbf{s}=[x, y, z, w, v_1]^T, \tag{14}$$

so that v_2 is excluded as redundant. Delayed-input targets use u_{i-d} with $d\geq 0$, where $d=0$ is the input applied in the interval immediately before the observation, and next-sample targets use u_{i+1}, which is not used to construct the predictor. After a washout of 500 samples, 5,499 predictor-target pairs remain and are divided chronologically, without shuffling, into 3,299 training, 1,100 validation and 1,100 test samples (60%, 20% and 20%). Standardisation uses training-subset means and standard deviations only, and the same test interval is used for all conditions with a given input seed.

Each target y is estimated by a ridge-regression readout (Hoerl & Kennard, 1970),

$$\hat{y}_i=\boldsymbol{\beta}^T\tilde{\boldsymbol{\xi}}_i+\beta_0, \qquad \min_{\boldsymbol{\beta},\beta_0} \|\mathbf{y}-\tilde{\mathbf{S}}\boldsymbol{\beta}-\beta_0\mathbf{1}\|_2^2+\alpha\|\boldsymbol{\beta}\|_2^2, \tag{15}$$

where $\tilde{\boldsymbol{\xi}}$ is the standardised state and $\alpha\in\{10^{-6},10^{-4},10^{-2},1,100\}$ is selected for each target by maximum validation R^2 and evaluated once on the test samples. Accuracy is measured by

$$R^2=1-\frac{\sum_i (y_i-\hat{y}_i)^2}{\sum_i (y_i-\bar{y})^2}, \qquad \mathrm{NRMSE}=\sqrt{1-R^2}, \tag{16}$$

with $\bar{y}$ the test-sample mean, so that $R^2\leq 0$ indicates no more information than a constant predictor. A linear readout of five features can represent at most five independent linear functions, so the linear memory capacity cannot exceed five.

Capacities are the test R^2 of readouts that reconstruct functions of the input history. Linear memory uses the targets u_{i-d} with $d=0,\ldots,50$. Nonlinear targets use delays $d=0,\ldots,10$: the second-order Legendre polynomial $P_2(u)=1/2\,(3u^2-1)$ and third-order polynomial $P_3(u)=1/2\,(5u^3-3u)$ of single delayed inputs, and the 55 pairwise products $u_{i-d_1}u_{i-d_2}$ with $d_1<d_2$. A target contributes to a capacity only if its test R^2 exceeds a threshold τ, defined for each simulation as the 99th percentile of the test R^2 obtained for the same targets after a random circular shift of at least 600 samples, which removes their relation to the state while preserving their statistics. With $C[\cdot]=R^2$ if $R^2>\tau$ and zero otherwise,

$$\mathrm{MC}=\sum_{d=0}^{50} C\,[u_{i-d}], \quad C_2=\sum C[P_2]+\sum C\left[u_{i-d_1}u_{i-d_2}\right], \quad C_3=\sum C[P_3], \tag{17}$$

and the total capacity is $C_{tot}=\mathrm{MC}+C_2+C_3$. The targets are not orthogonalised over the joint delay structure, so these are capacities of the specified target families and not a complete decomposition.

The primary benchmark is the NARMA-10 system-identification task, which requires memory and nonlinearity (Atiya & Parlos, 2000). With $u'_i=(u_i+1)/4\in[0,0.5]$,

$$y_{i+1}=0.3\,y_i+0.05\,y_i\sum_{j=0}^{9} y_{i-j}+1.5\,u'_{i-9}u'_i+0.1, \tag{18}$$

and the reservoir predicts y_{i+1} from ξ_i. As a control, the next input sample u_{i+1} is predicted; because the input is independent and identically distributed, no predictor can exceed $R^2=0$ on average, so this task checks that the pipeline does not manufacture skill. Reference predictors computed from the input alone on the same split are the training mean, persistence (for the next-sample task), a ridge readout on ten delayed inputs (linear delay line) and a ridge readout on those ten delays and all their pairwise products (quadratic delay line). The reservoir is judged to add predictive information only if it improves on the training mean and on the delay-line references consistently across conditions and input realisations.

The representations compared on the nominal-parameter conditions were the five-variable set, the raw six-variable set including v_2, each leave-one-variable-out set, the fast variables (x,y,z), the slow variables (w,v_1), and the five states augmented with all their products (20 features, a nonlinear-readout reference). Each was evaluated with the identical protocol. The effective dimension was quantified by the numerical rank of the standardised training feature matrix (singular values above 10^{-8} of the largest) and by the participation ratio

$$\mathrm{PR}=\frac{(\Sigma_k \lambda_k)^2}{\Sigma_k \lambda_k^2}, \tag{19}$$

where λ_k are the eigenvalues of the covariance of the standardised features. The comparison was restricted to regimes with non-zero capacity ($d\leq 0$).

For every operating regime and coupling, the conditional λ_1 was paired with MC, C_{tot} and NARMA-10 R^2, and the association was summarised by the Spearman rank correlation. Because conditions within a regime are not independent, the correlations are descriptive; they were supplemented by the variation of performance within regimes, by a class-resolved comparison of whether loss of chaos under perturbation restores performance, and by the variability across the five input realisations. The fraction of runs that remained bounded was reported as a separate reliability indicator.

All computations were implemented in Python and MATLAB for visual implementation.

RESULTS AND DISCUSSIONS

The reference operating point is the published parameter set with $d=0.46$ and κ between 0.01 and 0.20, with the initial condition $\mathbf{X}_0=(0.6,0.5,0.45,0.1,0.5,0.5)$. Table 1 defines the parameters and numerical protocol, and Table 2 defines the scenario set and data partition used throughout.

Table 1. Baseline parameters and numerical protocol used for the calculations.

Parameter	Value	Role
a	1.73	Linear coupling coefficient
b	−2.04	Nonlinear coupling coefficient
d	0.46 (varied: −0.4, −0.2, 0.0, 0.2, 0.35, 0.46)	Linear y-state coefficient; regime-defining coefficient
e_1, e_2	0.001, 0.005	Quadratic and quartic memory-

Parameter	Value	Role
		feedback strengths
f, g	0.67, 0.19	Linear and nonlinear inhibitory coupling
h	0.48	Linear excitation coefficient
j_1, j_2	0.8, 0.05	Quadratic and quartic nonlinear feedback coefficients
k	0.5	Linear feedback coefficient
n_1	1.0	Memory-state evolution parameter
X_0	(0.6, 0.5, 0.45, 0.1, 0.5, 0.5)	Initial condition
Input injection	x-equation, vector b = (1,0,0,0,0,0)	Input-coupling mechanism
Coupling κ	0.01, 0.05, 0.10, 0.20 (extended: 0.5, 1, 2, 4)	Input strength
Input	i.i.d. uniform on [−1, 1], 0.1 time units per sample	Excitation
Driven integration	DOP853, rtol 1e-10, atol 1e-12, max step 0.02	Reservoir trajectories
Lyapunov integration	RK4, h = 0.01, QR every 0.1	Spectrum

Table 2. Scenario set, simulation counts and data partition.

Item	Specification
Scenarios per regime and coupling	Nominal; parameters scaled by (1+δ), δ = ±0.01, ±0.05; initial state scaled by (1+δ), δ = ±0.01, ±0.05; looser numerical tolerance (10 in total)
Simulations	240 perturbation runs (seed 0); 96 nominal runs (seeds 1–4); 24 replica runs; 24 tight-tolerance runs; 12 strong-coupling runs
Input samples per run	6,000 (600 time units); 6,001 trajectory rows
Washout; aligned pairs	500; 5,499
Training / validation / test	3,299 / 1,100 / 1,100 (chronological)
Capacity targets	51 linear delays; 77 second- and third-order targets (delays 0–10)

The integrity of the trajectories is established first (Table 3). All 363 bounded trajectories were finite, had the expected length and satisfied equation (10) with E_{inv}=0 exactly, and the largest absolute state was 24.0. The zero error is structural, since v_1 and v_2 obey identical equations with identical initial values and are therefore advanced identically; the content of equation (8) was therefore also checked with

$v_1(0)-v_2(0)=0.1$, for which the difference was conserved to 2.0×10^{-15}. The invariant shows that v_2 is redundant and that the effective state dimension cannot exceed five, but it says nothing about whether a dynamical class or computational performance is preserved, which is examined in the remainder of this section.

Table 3. Numerical validation and integrity checks.

Check	Result	Interpretation
Bounded trajectories	363 of 384	21 runs escaped to infinity, all at $d\geq0.35$ with strong drive
Invariant error, equation (10)	0 (all bounded runs)	v_1-v_2 preserved
Invariant with offset 0.1	2.0×10^{-15}	Conservation holds for non-zero offset
Largest absolute state	24.0	Empirical bound over bounded runs
DOP853 (10^{-10}) versus tight reference at t = 10	2.9×10^{-14}	Converged at short horizon
RK4 versus tight reference at t = 10 (h = 0.02, 0.01, 0.005)	2.3×10^{-8}, 1.4×10^{-9}, 8.7×10^{-11}	Fourth-order convergence
Divergence above 10^{-2} within 60 time units	none	Reference agreement at short horizon
λ_1 at h = 0.01 versus 0.02 (d=0.46)	0.080 versus 0.081	Insensitive to step size
λ_1 at h = 0.01 versus 0.02 (d=0.35)	0.096 versus 0.102	Within block standard errors

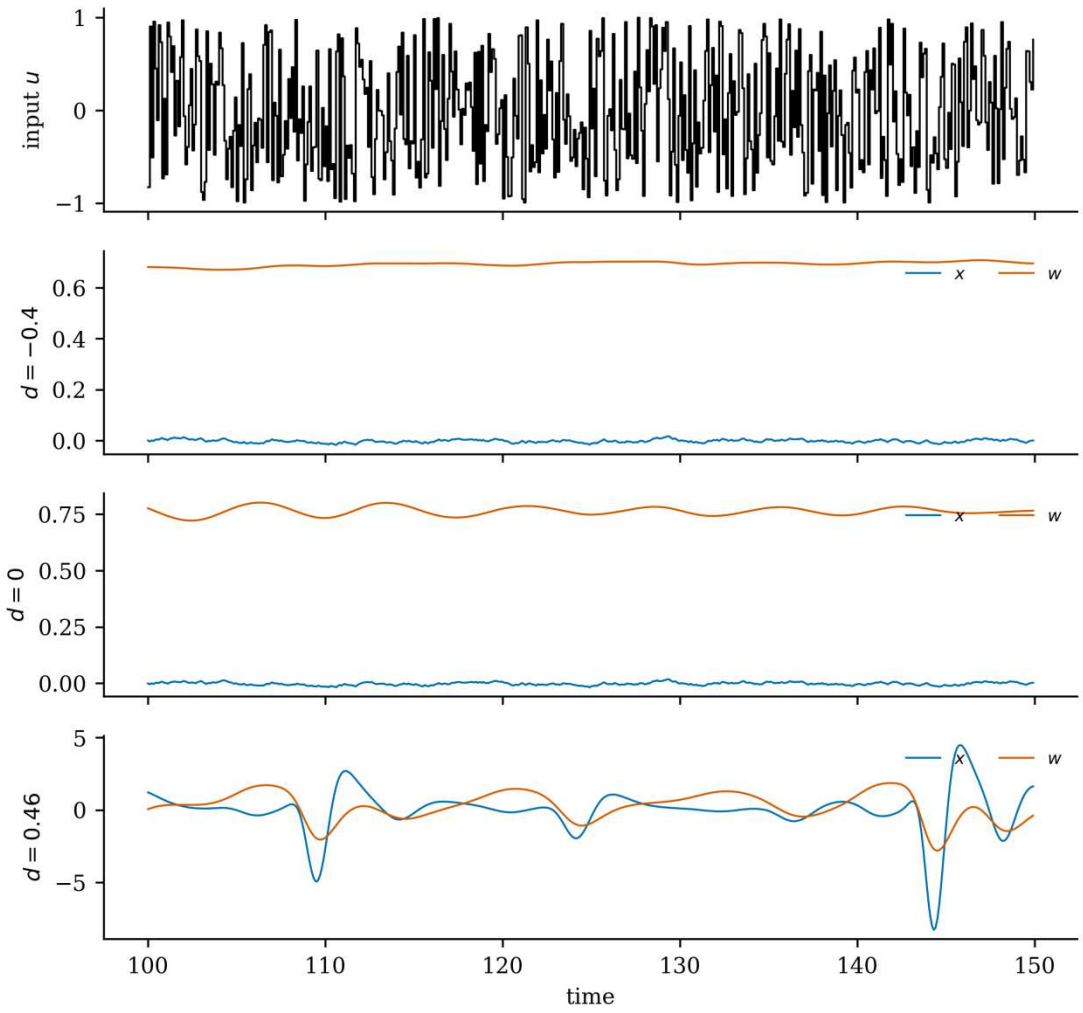


Figure 1. Input sequence and the resulting x and w responses for three regimes at κ=0.05 (time 100 to 150). For d=−0.4 the response follows the input history; for d=0.46 the response is dominated by internal chaotic motion.

Figure 1 illustrates the contrast on which the remaining results are built. For d=−0.4 the state is a smooth, filtered image of the input, with w integrating it; for d=0.46 the irregular chaotic oscillation of x dominates and the weak input is not visible in the trace. The regimes were identified quantitatively from the Lyapunov spectrum. Sweeping d (Figure 2) shows a non-chaotic range for $d \leq 0.25$, the onset of chaos between d=0.25 and d=0.30, chaos with a single positive exponent up to d=0.50, and unbounded trajectories at d=0.55. At the published coefficient (d=0.46) the leading exponent is λ_1=0.080±0.011 (two standard errors) and λ_2=0.0006 is indistinguishable from zero, so the regime is chaotic with one positive exponent and is not hyperchaotic. This agrees with the value λ_1=0.0824 and the single positive exponent reported for the same system by Ajayi (2026) and confirms that the baseline of the present study is the established regime. For d<0 the vanishing leading exponents reflect the manifold of equilibria (x=y=z=0 with arbitrary w, v_1 and v_2), on which w and v_1 act as integrators of the input, together with strongly contracting fast directions; for d=0.2 the exponent λ_1 is small but positive (0.001 to 0.003, below the zero band), so this regime is marginal and not strongly contracting.

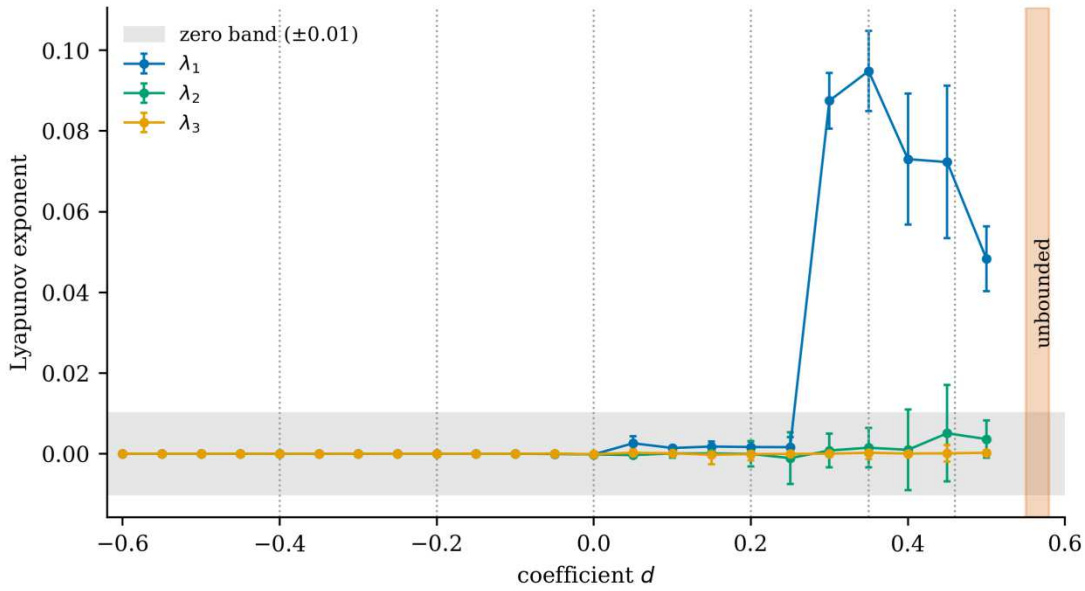


Figure 2. Lyapunov exponents λ_1 to λ_3 of the autonomous system versus the coefficient d (error bars ±2 SE; grey band: zero band ±0.01). Vertical dotted lines mark the six operating regimes. For $d \geq 0.55$ trajectories are unbounded.

Table 4. Autonomous Lyapunov classification and its retention across the ten scenarios.

d	Nominal λ1 (±2 SE)	Nominal λ2	Class	Class retained	Scenarios with class change	λ1 range over scenarios
-0.4	0.0000 ± 0.0000	0.0000	non-chaotic	10/10	–	0.0000 to 0.0000
-0.2	-0.0000 ± 0.0000	0.0000	non-chaotic	10/10	–	-0.0000 to 0.0000
0.0	-0.0001 ± 0.0002	0.0001	non-chaotic	10/10	–	-0.0004 to 0.0002
0.2	0.0011 ± 0.0005	-0.0002	non-chaotic	10/10	–	0.0010 to 0.0015
0.35	0.0963 ± 0.0140	0.0014	chaotic	8/10	Param+0.05, Init+0.05	0.0004 to 0.1020
0.46	0.0801 ± 0.0111	0.0006	chaotic	9/10	Param-0.05	0.0047 to 0.0848

The retention of the classification under perturbation (Table 4, Figure 3) answers the first objective quantitatively. In the four non-chaotic regimes the classification was retained in all ten scenarios, and λ_1 varied by less than 5×10^{-4}. In the chaotic regimes retention was incomplete: at d=0.46 nine of ten scenarios remained chaotic, the exception being the −5% simultaneous parameter perturbation (λ_1=0.0047±0.0036), and at d=0.35 eight of ten were retained, the exceptions being the +5% parameter and +5% initial-state perturbations ($\lambda_1 \approx 0.0004$ to 0.0007). The ±1% perturbations never changed the class. Loss of chaos for a 5% change of the initial state at d=0.35 shows that this regime is multistable on that scale, so that a single trajectory does not

determine the regime. For any zero band between 0.005 and 0.05 the classes are unchanged, except that the d=0.46, −5% case is borderline at the lower end. Retention of the dynamical class therefore depends on the size and type of the perturbation: it is complete at ±1%, partial at ±5% and depends on the regime.

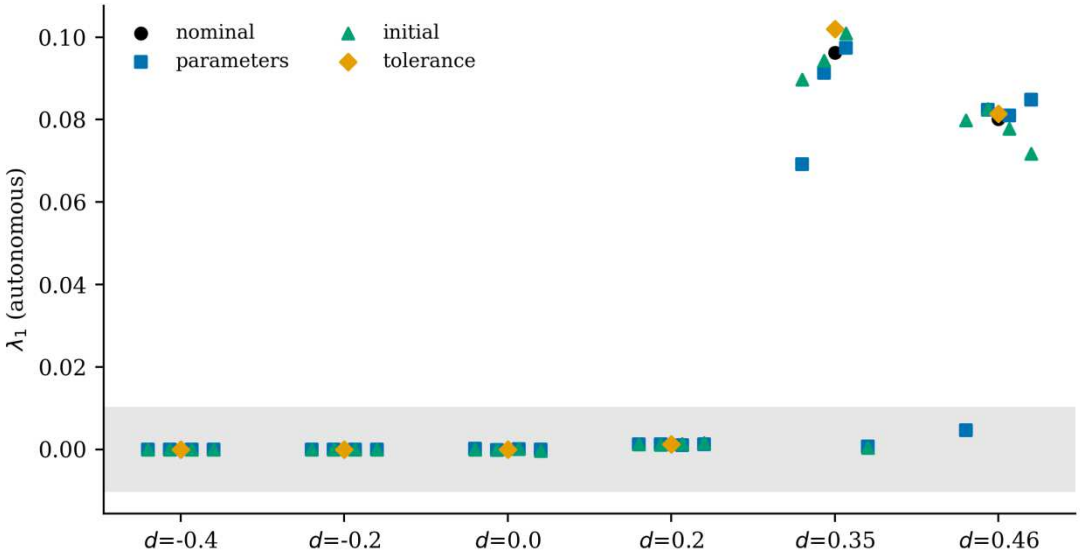


Figure 3. Autonomous λ_1 for the ten scenarios of each regime. The grey band is the zero band. Loss of the chaotic class occurs only for ±5% perturbations.

Because the input is additive, the conditional exponents under drive remain close to the autonomous values (Table 5): chaos is retained at d=0.35 and d=0.46 for $\kappa \leq 0.1$ (with λ_1 reduced from 0.10 to about 0.06 at d=0.35 for $\kappa \geq 0.1$), and the non-chaotic regimes stay non-chaotic. The driven chaotic system is, however, not always bounded (Table 6). At d=0.46 the number of input realisations that escaped to infinity was 0, 1, 3 and 4 of 5 for κ=0.01,0.05,0.10,0.20, and one of five at d=0.35 and κ=0.20; all ten scenarios at d=0.46, κ=0.20 and two at κ=0.10 were unbounded, so that the conditional spectrum at d=0.46, κ=0.20 could not be computed. No unbounded run occurred for $d \leq 0.2$. Boundedness of the driven chaotic reservoir therefore depends on the input realisation and the coupling, which is a reliability limit that is invisible in the autonomous classification.

Table 5. Conditional leading Lyapunov exponent λ_1 along the driven trajectory (input realisation 0).

d	κ=0.01	κ=0.05	κ=0.1	κ=0.2
-0.4	-0.0000	-0.0000	-0.0000	-0.0000
-0.2	-0.0000	-0.0000	-0.0000	0.0001
0.0	-0.0000	0.0002	-0.0000	-0.0002
0.2	0.0015	0.0018	0.0017	0.0027
0.35	0.0993	0.1011	0.0615	0.0596
0.46	0.0782	0.0848	0.0845	unbounded

Table 6. Number of unbounded runs out of five input realisations (nominal parameters).

d	κ=0.01	κ=0.05	κ=0.1	κ=0.2
-0.4	0/5	0/5	0/5	0/5
-0.2	0/5	0/5	0/5	0/5
0.0	0/5	0/5	0/5	0/5
0.2	0/5	0/5	0/5	0/5
0.35	0/5	0/5	0/5	1/5
0.46	0/5	1/5	3/5	4/5

The numerical convergence of the trajectories is summarised in Figure 4 and Table 7. At short horizons the integration is converged far below the scale of the state (Table 3). Over the full 600 time units the behaviour depends on the regime. In the four regimes with $d \leq 0.2$, trajectories computed with different tolerances or from a 10^{-8}-perturbed initial state never separated by more than 10^{-2}. In the chaotic regimes all perturbed trajectories separated at a finite time: after 334 to 357 time units for tolerance changes (initial discrepancy of order 10^{-13}) and after 134 to 142 time units for the 10^{-8} replica. These horizons agree with the exponent: with $\lambda_1 \approx 0.08$, an error growing from 10^{-8} to 10^{-2} is expected after $\ln(10^6)/\lambda_1 \approx 170$ time units, and from about 10^{-13} after about 320. Pointwise chaotic trajectories are therefore reproducible only up to a finite horizon, whereas the Lyapunov estimates were insensitive to step size and settled with integration time (Figure 4a). This is the distinction on which the study relies: classification and statistical quantities converge, whereas individual chaotic trajectories do not, and numerical convergence is therefore a prerequisite for, and is established before, the computational assessment.

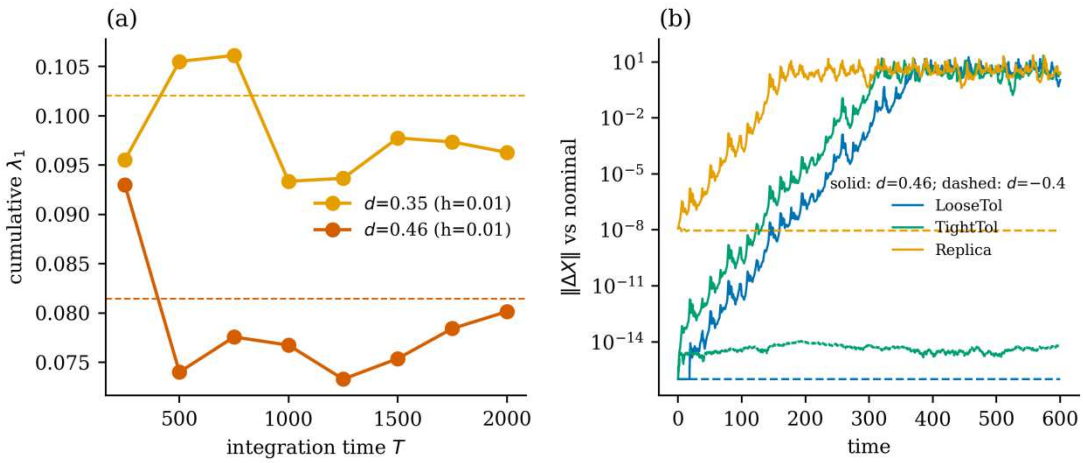


Figure 4. Numerical convergence. (a) Cumulative λ_1 versus integration time for d=0.35 and d=0.46 (dashed: h=0.02 estimate). (b) Distance between the nominal trajectory and the loose-tolerance, tight-tolerance and initial-state replica trajectories (κ=0.05); solid: d=0.46, dashed: d=−0.4.

Table 7. Median divergence time t_{div} (time units; first $\|\Delta X\|_2 > 10^{-2}$) of the nominal trajectory from recomputed variants, over the four couplings; n is the number of conditions that diverged out of those bounded.

d	Loose tolerance (1e-8)	Tight tolerance (1e-12)	Initial replica (1e-8)
-0.4	no divergence	no divergence	no divergence
-0.2	no divergence	no divergence	no divergence
0.0	no divergence	no divergence	no divergence
0.2	no divergence	no divergence	no divergence
0.35	351 (n=4/4)	334 (n=4/4)	142 (n=4/4)
0.46	357 (n=2/2)	344 (n=3/3)	134 (n=3/3)

Linear memory depends strongly on the regime and weakly on the coupling (Table 8, Figure 5). In the non-chaotic regimes with $d \leq 0$ the readout recovers delayed inputs over tens of samples: MC is 2.60±0.27 to 2.42±0.21 at $d=-0.4$, 2.19±0.22 to 2.09±0.23 at $d=-0.2$ and 0.96±0.11 to 1.10±0.18 at $d=0$ for κ from 0.01 to 0.20, against a ceiling of five. By contrast MC is zero within the surrogate threshold (at most 0.011) at $d=0.2$ and in both chaotic regimes at all four couplings. Within a regime the effect of κ is of the same size as the variation between input realisations (standard deviation 0.1 to 0.27), so only trends are reported: a slight decrease with κ for $d \leq -0.2$ and a slight increase for $d=0$. The insensitivity to small κ is expected because the response of the non-chaotic regimes is nearly linear and the standardised readout removes the overall scale. The memory that is present is carried by the integrating variables (w, v_1) and the fast variables, and is limited by the number of readout features and not by the delay range examined. The absence of memory in the chaotic regimes follows from the positive conditional exponent: the state is dominated by internal chaotic motion that has no fading dependence on the weak input, so a linear readout of five features finds no input information although the trajectories are finite and satisfy the invariant. The presence of complex dynamics therefore does not imply memory capacity; in this system the capacity is absent precisely where the dynamics are chaotic.

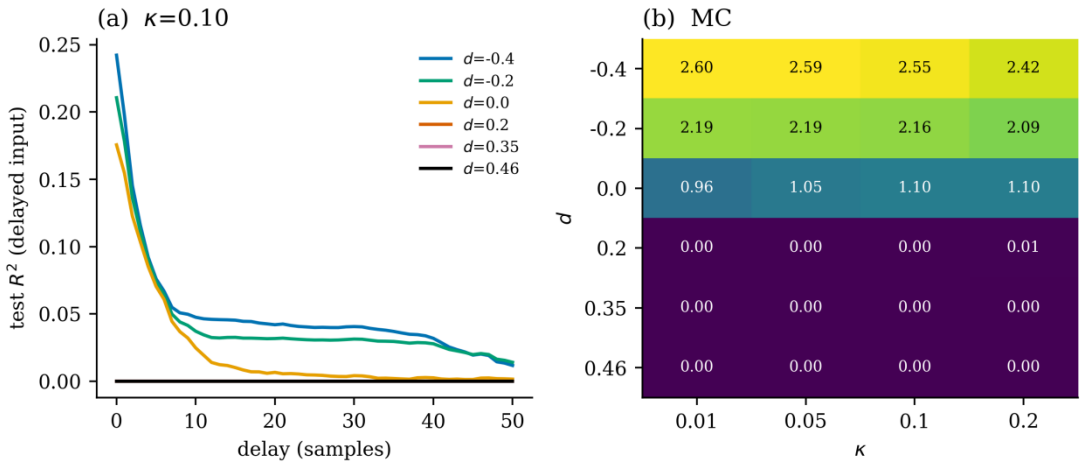


Figure 5. (a) Test R^2 of delayed-input reconstruction versus delay at $\kappa=0.10$, averaged over input realisations. (b) Linear memory capacity MC for each regime and coupling (mean over input realisations).

d	κ	valid seeds	MC	C2	C3	NARMA-10 R^2	next-sample R^2
-0.4	0.01	5	2.596 ± 0.267	0.000 ± 0.001	0.000 ± 0.000	0.488 ± 0.029	-0.002 ± 0.003
-0.4	0.05	5	2.589 ± 0.246	0.000 ± 0.000	0.000 ± 0.000	0.487 ± 0.029	-0.002 ± 0.003
-0.4	0.1	5	2.554 ± 0.223	0.000 ± 0.001	0.000 ± 0.000	0.486 ± 0.028	-0.002 ± 0.003
-0.4	0.2	5	2.421 ± 0.214	0.000 ± 0.000	0.000 ± 0.000	0.479 ± 0.029	-0.001 ± 0.002
-0.2	0.01	5	2.193 ± 0.222	0.005 ± 0.007	0.000 ± 0.000	0.486 ± 0.030	-0.001 ± 0.002
-0.2	0.05	5	2.189 ± 0.207	0.003 ± 0.005	0.000 ± 0.000	0.485 ± 0.030	-0.001 ± 0.003
-0.2	0.1	5	2.165 ± 0.197	0.000 ± 0.001	0.000 ± 0.000	0.486 ± 0.030	-0.001 ± 0.003
-0.2	0.2	5	2.090 ± 0.228	0.000 ± 0.000	0.000 ± 0.000	0.484 ± 0.031	-0.001 ± 0.003
0.0	0.01	5	0.957 ± 0.110	0.003 ± 0.004	0.001 ± 0.001	0.466 ± 0.028	-0.002 ± 0.003
0.0	0.05	5	1.046 ± 0.117	0.002 ± 0.005	0.000 ± 0.000	0.480 ± 0.030	-0.002 ± 0.003
0.0	0.1	5	1.102 ± 0.142	0.004 ± 0.006	0.000 ± 0.000	0.481 ± 0.029	-0.001 ± 0.002
0.0	0.2	5	1.099 ± 0.178	0.000 ± 0.001	0.000 ± 0.000	0.474 ± 0.032	-0.002 ± 0.002
0.2	0.01	5	0.000 ± 0.000	0.004 ± 0.009	0.000 ± 0.000	-0.033 ± 0.024	-0.003 ± 0.003
0.2	0.05	5	0.000 ± 0.000	0.009 ± 0.011	0.000 ± 0.000	-0.029 ± 0.020	-0.003 ± 0.003
0.2	0.1	5	0.001 ± 0.002	0.005 ± 0.011	0.000 ± 0.000	-0.033 ± 0.020	-0.002 ± 0.001
0.2	0.2	5	0.011 ± 0.025	0.001 ± 0.001	0.000 ± 0.000	-0.023 ± 0.037	-0.004 ± 0.002
0.35	0.01	5	0.001 ± 0.003	0.000 ± 0.000	0.000 ± 0.000	-0.037 ± 0.032	-0.003 ± 0.002
0.35	0.05	5	0.000 ± 0.000	0.006 ± 0.012	0.002 ± 0.005	-0.052 ± 0.021	-0.005 ± 0.002
0.35	0.1	5	0.000 ± 0.000	0.000 ± 0.000	0.000 ± 0.000	-0.025 ± 0.027	-0.002 ± 0.002
0.35	0.2	4	0.000 ± 0.000	0.000 ± 0.000	0.000 ± 0.000	-0.016 ± 0.019	-0.003 ± 0.002
0.46	0.01	5	0.001 ± 0.003	0.003 ± 0.006	0.000 ± 0.000	-0.033 ± 0.031	-0.003 ± 0.004

d	κ	valid seeds	MC	C2	C3	NARMA-10 R^2	next-sample R^2
0.46	0.05	4	0.000 ± 0.000	0.000 ± 0.000	0.000 ± 0.000	-0.030 ± 0.018	-0.004 ± 0.001
0.46	0.1	2	0.000 ± 0.000	0.000 ± 0.000	0.000 ± 0.000	-0.042 ± 0.009	-0.005 ± 0.000
0.46	0.2	1	0.000	0.000	0.000	-0.041	-0.004

Table 8. Capacities and prediction scores (mean ± SD over the valid input realisations; "valid seeds" excludes unbounded runs).

No nonlinear capacity was demonstrated by the dynamics within the specified target families. The quadratic capacity C_2 and the cubic capacity C_3 were at or below 0.01 in every condition (Table 8) and never exceeded 0.013 in the supplementary strong-coupling runs (κ=0.5 to 4; Table 9, Figure 6b), in which MC itself fell from about 2.05 to 1.5 at d=−0.4 and collapsed to zero at d=0 for $\kappa \geq 2$ while the state amplitude rose to 24.8. Stronger drive therefore moved the state into larger excursions without producing usable nonlinear transformations. In the non-chaotic regimes the nonlinear terms of the model are small because the states remain below about 1 and the coefficients e_1 and e_2 are small, and in the chaotic regimes the state is too weakly related to the input for any function of the input to be recovered. The nonlinear capacity that is available is created by the readout and not stored in the dynamics: augmenting the five states with their pairwise products gave a mean C_2=0.86, against 0.001 for the five states, over the non-chaotic nominal conditions with $d \leq 0$ (Table 10, Figure 6a), with the total capacity rising from 2.14 to 3.04. This reflects a quadratic readout acting on retained linear memory and should not be read as nonlinear information processing by the memcapacitive dynamics.

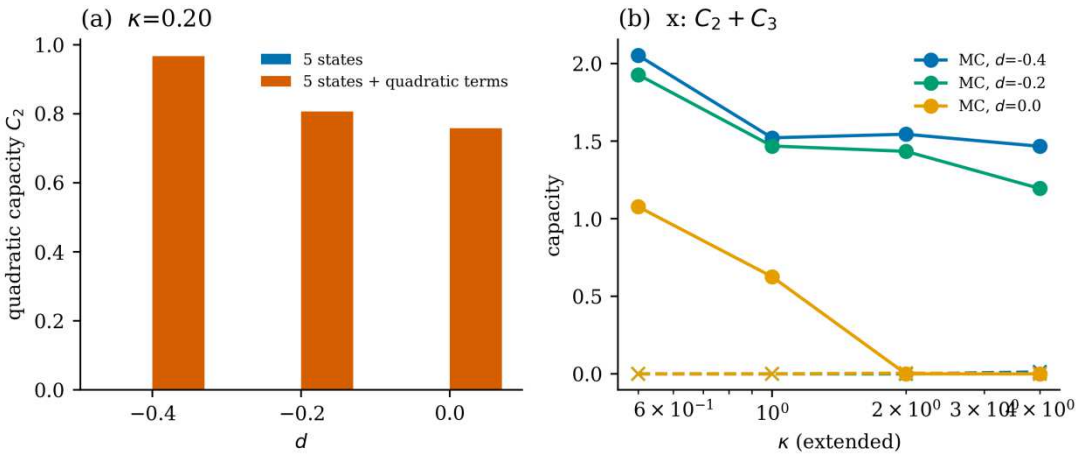


Figure 6. (a) Quadratic capacity C_2 at κ=0.20 for the five-state readout and for the five states augmented with quadratic terms. (b) Strong-coupling runs: MC (circles) and C_2+C_3 (crosses).

Table 9. Strong-coupling runs (non-chaotic regimes, input realisation 0).

d	κ	Bounded	MC	C2	C3	NARMA-10 R^2	Max abs state
-0.4	0.5	yes	2.053	0.0	0.0	0.471	1.462

d	κ	Bounded	MC	C2	C3	NARMA-10 R²	Max abs state
-0.4	1.0	yes	1.522	0.0	0.0	0.389	1.899
-0.4	2.0	yes	1.545	0.0	0.0	0.417	2.105
-0.4	4.0	yes	1.467	0.013	0.0	0.458	2.656
-0.2	0.5	yes	1.929	0.0	0.0	0.515	1.351
-0.2	1.0	yes	1.469	0.0	0.0	0.48	1.707
-0.2	2.0	yes	1.434	0.0	0.0	0.501	2.18
-0.2	4.0	yes	1.195	0.0	0.0	0.466	4.145
0.0	0.5	yes	1.077	0.0	0.0	0.501	1.472
0.0	1.0	yes	0.627	0.0	0.0	0.348	1.941
0.0	2.0	yes	0.0	0.0	0.005	-2.971	5.079
0.0	4.0	yes	0.0	0.0	0.0	-0.064	24.795

The effective computational dimension of the state is smaller than its nominal dimension (Table 10, Figure 7). The numerical rank of the raw six-variable representation was five: including v_2 changed neither MC (2.134 against 2.135) nor NARMA-10 R^2. The reduction does not stop there. Omitting y, w or v_1 changed MC by less than 0.04, the fast variables (x,y,z) alone reached MC 2.23 and NARMA-10 R^2 0.522, equal to the full five-variable set, and the slow variables (w,v_1) alone gave only MC 0.59. The injected variable x was indispensable: removing it reduced MC from 2.14 to 0.99 and NARMA-10 R^2 from 0.52 to 0.12, and removing z reduced MC to 1.65. For the regimes with capacity the useful computational dimension is therefore about three, with x and z carrying most of the information, compared with six nominal coordinates, five after the invariant and a participation ratio of 3.2 for the five-variable set. This conclusion applies to the non-chaotic regimes (d≤0), where there is capacity to apportion, and depends on the injection channel.

Table 10. Alternative state representations (mean over the 12 non-chaotic nominal conditions with d≤0; MC, C_2 and NARMA-10 R^2 are test values).

Representation	Features	Numerical rank	Participation ratio	MC	C2	NARMA-10 R²
full5	5	5.0	3.16	2.135	0.001	0.522
raw6_with_v2	6	5.0	2.924	2.134	0.001	0.522
minus_x	4	4.0	2.467	0.988	0.001	0.116
minus_y	4	4.0	2.842	2.122	0.001	0.523
minus_z	4	4.0	2.544	1.647	0.003	0.493
minus_w	4	4.0	3.364	2.124	0.001	0.522
minus_v1	4	4.0	2.941	2.169	0.002	0.521
fast3_xyz	3	3.0	2.556	2.225	0.001	0.522
slow2_w_v1	2	2.0	1.381	0.589	0.0	0.076
quad_expanded 5	20	19.75	5.816	2.174	0.862	0.534

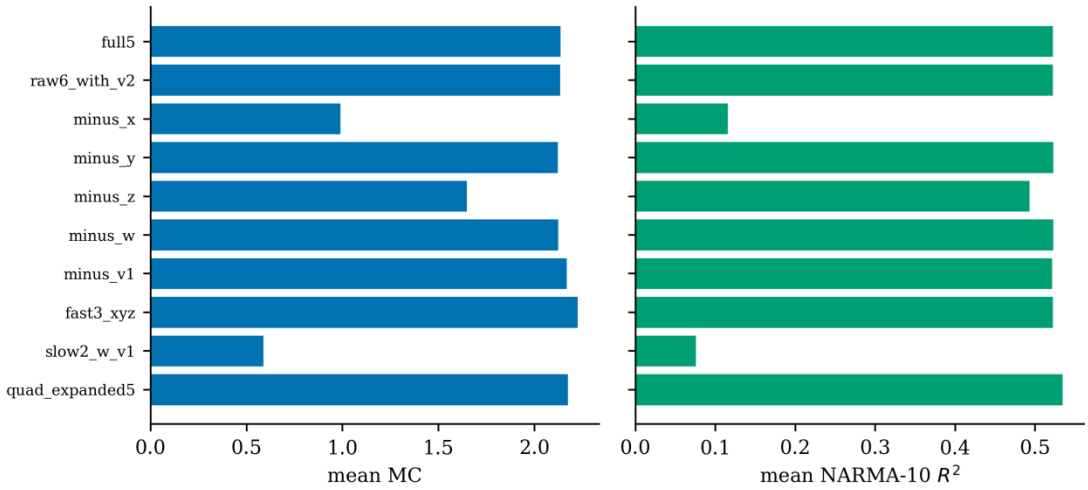


Figure 7. Mean linear memory capacity and NARMA-10 test R^2 for alternative state representations ($d \leq 0$ conditions).

Prediction performance was assessed against reference predictors (Table 11, Figure 8). For the i.i.d. next-sample control the reservoir test R^2 was between −0.005 and −0.001 in all regimes, indistinguishable from the training mean (−0.002±0.002) and the delay-line references (−0.005 and −0.012), while persistence gave −0.937±0.061. This is the expected ceiling for white noise, so near-zero next-sample scores reflect the task and not a failed reservoir; it also means that next-sample prediction of an i.i.d. input cannot discriminate between reservoirs and was not used for inference. On the NARMA-10 benchmark, the regimes with memory reached R^2 between 0.466 and 0.488 ($d \leq 0$, all couplings; standard deviation 0.03 over input realisations), far above the training mean (−0.023±0.022). The reservoir did not, however, outperform simple input-only references: the linear delay line scored 0.660±0.024 and the quadratic delay line 0.739±0.021, so the five-state reservoir is a poorer predictor than a ridge model on the last ten inputs, and the best score obtained by adding quadratic terms to the readout (0.534) did not close the gap. In the chaotic regimes and at d=0.2 the scores were −0.016 to −0.052, equivalent to or worse than predicting the mean. Prediction performance therefore varies strongly with the operating condition and is not determined by the dynamical class alone, since the non-chaotic regime d=0.2 shows no skill. The data support weak but real predictive information in the non-chaotic regimes and do not support a predictive advantage over simpler models.

Table 11. Reference predictors on the same test intervals (mean ± SD over five input realisations).

Task	baseline	R^2
NARMA10	LinearDelayLine(10)	0.660 ± 0.024

Task	baseline	R^2
NARMA10	QuadraticDelayLine(10)	0.739 ± 0.021
NARMA10	TrainingMean	-0.023 ± 0.022
NextSample	LinearDelayLine(10)	-0.005 ± 0.004
NextSample	Persistence	-0.937 ± 0.061
NextSample	QuadraticDelayLine(10)	-0.012 ± 0.005
NextSample	TrainingMean	-0.002 ± 0.002

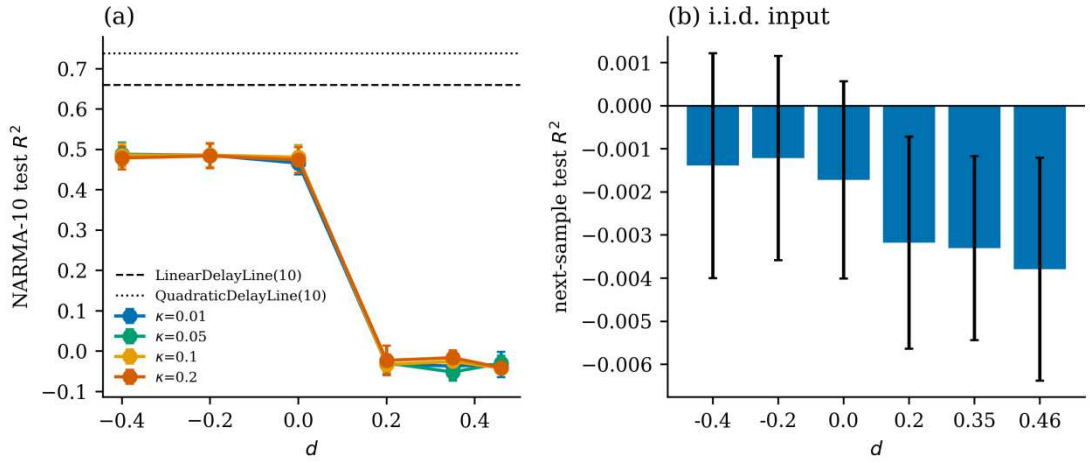


Figure 8. (a) NARMA-10 test R^2 versus d for each coupling (mean ± SD over input realisations); dashed and dotted lines are the linear and quadratic delay-line references. (b) Next-sample test R^2 for the i.i.d. input (control task).

Dynamical reliability and computational performance were compared on the same conditions (Figure 9). Across the 22 bounded nominal conditions the conditional λ_1 was strongly and negatively associated with the computational scores (Spearman ρ=−0.76 for MC, −0.77 for C_{tot} and −0.72 for NARMA-10 R^2; $p<2\times10^{-4}$), and the association over the 228 bounded perturbation scenarios was similar (ρ=−0.77 and −0.74). These coefficients are descriptive because the points cluster by regime, and three observations show that the two properties are related but distinct. First, non-chaotic dynamics are necessary but not sufficient for capacity: the regime d=0.2 is non-chaotic in all ten scenarios and at every coupling, yet its MC is at most 0.05 and its NARMA-10 R^2 is negative. Second, loss of chaos does not restore performance: the 11 bounded scenarios of the chaotic regimes that were classified non-chaotic had mean MC 0.002 and NARMA-10 R^2 of −0.014, against 0.002 and −0.012 for the 57 that stayed chaotic. Third, retention of the class does not guarantee retention of performance: at d=0 the class was retained in all ten scenarios, yet MC ranged from 0.43 to 1.42 and NARMA-10 R^2 from 0.16 to 0.52, whereas performance varied little within the best regime (MC 2.59 to 2.95 at d=−0.4). Reliable dynamics therefore coincide with useful computation in the contracting regimes with integrator states ($d\leq0$, bounded in all realisations) and do not coincide in the marginal regime (d=0.2) or in the chaotic regimes, where bounded, classification-retaining dynamics can be accompanied by zero capacity and, at stronger drive, by loss of boundedness.

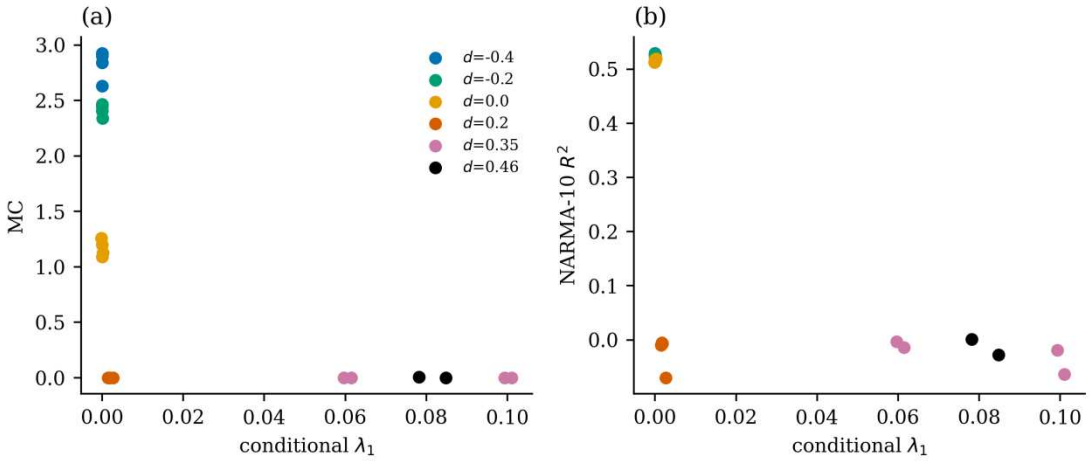


Figure 9. Conditional λ_1 versus (a) MC and (b) NARMA-10 test R^2 for the 22 bounded nominal conditions, coloured by regime.

Table 12 relates the aim and objectives to the evidence. Each objective is answered by a measured quantity, and the answers include negative findings: the study establishes that the system provides linear memory in contracting regimes and does not provide demonstrable nonlinear capacity or a predictive advantage over simple references. The research gap is therefore filled in the sense that the connection between numerical reliability, dynamical-regime retention, memory, nonlinear processing, effective dimension and prediction is now quantified on matched conditions, and the quantified answer is that the connection is a dissociation and not an identity.

Table 12. Aim and objectives and the evidence that answers them.

Objective	Evidence	Outcome
(i) Numerical convergence and class retention	Tables 3, 4, 7; Figures 2–4	Integration converged at short horizons; chaotic trajectories diverge after 134–357 time units while exponents are step-size insensitive; class retained 10/10 (non-chaotic), 9/10 and 8/10 (chaotic), lost only at ±5%
(ii) Input-driven formulation	Equation (9); Tables 1–2	Additive injection into x, state vector (x, y, z, w, v_1), ridge readout
(iii) Linear and nonlinear capacity	Tables 8–9; Figures 5–6	MC up to 2.6 for $d \leq 0$, zero for $d \geq 0.2$; C_2 and $C_3 \leq 0.013$
(iv) State representations	Table 10; Figure 7	Rank 5 of 6; (x, y, z) match all five; x essential
(v) Out-of-sample prediction	Table 11; Figure 8	NARMA-10 R^2 0.47–0.49 for $d \leq 0$; below delay-line references (0.66, 0.74)
(vi) Reliability versus performance	Tables 5–6; Figure 9	$\rho \approx -0.76$; d = 0.2 and perturbation analysis show dissociation

Several limitations qualify these conclusions. They apply to the specified model, the additive injection into *x*, the five-state linear ridge readout, i.i.d. uniform excitation and a sampling interval of 0.1 time units; other injection channels were found to be bounded only at weak coupling in the exploratory runs and were not explored further.

The regimes were produced by changing the single coefficient d, and the perturbation scenarios were evaluated for one input realisation, with five realisations used only for the nominal parameters. The Lyapunov classification depends on the zero band and on finite-time estimates, and the marginal regime d=0.2 has a small positive λ_1 below that band. The linear memory capacity is bounded by the five features, so low capacity may partly reflect the small readout. The simulation is noiseless, and physical noise, component tolerances and circuit-level effects are not modelled; no claim is made about hardware reservoir computing.

CONCLUSION

This research investigated whether the six-dimensional series-connected memcapacitor system can serve as a numerically reliable, input-driven computational substrate, and how its computational performance relates to the retention of its dynamical regime. The results answer the six objectives as follows. First, the integrations are converged at short horizons and the Lyapunov exponents are insensitive to step size, whereas individual chaotic trajectories diverge after 134 to 357 time units, as expected from $\lambda_1 \approx 0.08$. The published coefficients give a chaotic regime with a single positive exponent ($\lambda_1 = 0.080 \pm 0.011$), in agreement with the earlier dynamical study; this classification was retained in 9 of 10 and 8 of 10 scenarios in the two chaotic regimes, was lost only under ±5% perturbations, and was retained in every scenario of the non-chaotic regimes, while the driven chaotic system escaped to infinity in four of five input realisations at the strongest coupling. Second, the input-driven formulation with injection into x, the observable state (x,y,z,w,v_1) and a ridge readout provided a reproducible measurement architecture. Third, linear memory capacity up to 2.6 was present only in the non-chaotic regimes with integrator states and was zero in the chaotic regimes and in the marginal regime d=0.2, and no nonlinear capacity was found in the dynamics at any coupling examined. Fourth, the six coordinates reduce to five by the invariant and to about three useful ones, with x essential. Fifth, the reservoir predicted the NARMA-10 benchmark with R^2 of 0.47 to 0.49 in the memory-bearing regimes, better than the mean but below a linear delay-line reference (0.66), and showed no skill on an i.i.d. next-sample control, as expected for white noise. Sixth, dynamical reliability and computational usefulness were related (Spearman $\rho \approx -0.76$) but distinct: chaotic complexity coincided with the absence of capacity, yet absence of chaos did not by itself guarantee capacity, and retention of the dynamical class did not guarantee retention of performance. The research gap is thereby addressed: the connection between numerical reliability, dynamical-regime retention, memory, nonlinear processing, effective dimension and prediction has been quantified on matched conditions. For the intended application, the memcapacitive system is a usable linear-memory substrate in its contracting regime but not a demonstrated nonlinear reservoir.

DECLARATIONS

Funding: The research received no specific grant from any funding agency or public.

Clinical Trial Registration: This research does not involve a clinical trial.

Ethics Approval: Not Applicable

Competing Interest: The author declares there is no competing interest as regards this research

Author Contribution: I. O. Ajayi conceived the study, developed and designed the computational framework, carried out the numerical simulations, analyzed and interpreted the results, prepared the figures, wrote and revised the manuscript and approved the final version for publication.

Code Availability: The Python codes used for the numerical simulations and visualization are available from the corresponding author upon request.

Data Availability: The datasets generated and analyzed during this research are available from the corresponding author upon reasonable request.

Clinical Trail Number: Not applicable.

Consent to Publish declaration: Not applicable.

Consent to Participate declaration: Not applicable.

REFERENCES

Adelakun, A. O., Egunjobi, A. I., & Adeyeri, J. A. (2026). Hyperchaos in a series-connected memcapacitor system. Discover Electronics, 3, Article 85. https://doi.org/10.1007/s44291-026-00236-5

Ajayi, I. O. (2026). Chaotic dynamics, basin structure and global dynamical analysis of a six-dimensional series memcapacitor system. Discover Electronics, 3, Article 147. https://doi.org/10.1007/s44291-026-00297-6

Atiya, A. F., & Parlos, A. G. (2000). New results on recurrent network training: Unifying the algorithms and accelerating convergence. IEEE Transactions on Neural Networks, 11(3), 697–709.

Benettin, G., Galgani, L., Giorgilli, A., & Strelcyn, J.-M. (1980). Lyapunov characteristic exponents for smooth dynamical systems and for Hamiltonian systems; a method for computing all of them. Part 1: Theory. Meccanica, 15, 9–20.

Brzeski, P., Lazarek, M., Kapitaniak, T., Kurths, J., & Perlikowski, P. (2016). Basin stability approach for quantifying responses of multistable systems with parameters mismatch. Meccanica, 51, 2713–2726. https://doi.org/10.1007/s11012-016-0534-8

Dambre, J., Verstraeten, D., Schrauwen, B., & Massar, S. (2012). Information processing capacity of dynamical systems. Scientific Reports, 2, Article 514. https://doi.org/10.1038/srep00514

Di Ventra, M., Pershin, Y. V., & Chua, L. O. (2009). Circuit elements with memory: Memristors, memcapacitors, and meminductors. Proceedings of the IEEE, 97(10), 1717–1724. https://doi.org/10.1109/JPROC.2009.2021077

Dormand, J. R., & Prince, P. J. (1980). A family of embedded Runge–Kutta formulae. Journal of Computational and Applied Mathematics, 6(1), 19–26.

Gauthier, D. J., Bollt, E., Griffith, A., & Barbosa, W. A. S. (2021). Next generation reservoir computing. Nature Communications, 12, Article 5564. https://doi.org/10.1038/s41467-021-25801-2

Hairer, E., Nørsett, S. P., & Wanner, G. (1993). Solving ordinary differential equations I: Nonstiff problems (2nd ed.). Springer.

Hoerl, A. E., & Kennard, R. W. (1970). Ridge regression: Biased estimation for nonorthogonal problems. Technometrics, 12(1), 55–67.

Inubushi, M., & Yoshimura, K. (2017). Reservoir computing beyond the memory-nonlinearity trade-off. Scientific Reports, 7, Article 10199. https://doi.org/10.1038/s41598-017-10257-6

Liang, X., Tang, J., Zhong, Y., Gao, B., Qian, H., & Wu, H. (2024). Physical reservoir computing with emerging electronics. Nature Electronics, 7, 193–206. https://doi.org/10.1038/s41928-024-01133-z

Lukoševičius, M., & Jaeger, H. (2009). Reservoir computing approaches to recurrent neural network training. Computer Science Review, 3(3), 127–149. https://doi.org/10.1016/j.cosrev.2009.03.005

Menck, P. J., Heitzig, J., Marwan, N., & Kurths, J. (2013). How basin stability complements the linear-stability paradigm. Nature Physics, 9, 89–92. https://doi.org/10.1038/nphys2516

Skokos, C. (2010). The Lyapunov characteristic exponents and their computation. In J. Souchay & R. Dvorak (Eds.), Dynamics of small solar system bodies and exoplanets (Lecture Notes in Physics, Vol. 790, pp. 63–135). Springer. https://doi.org/10.1007/978-3-642-04458-8_2

Stepney, S. (2024). Physical reservoir computing: A tutorial. Natural Computing, 23, 665–685. https://doi.org/10.1007/s11047-024-09997-y

Tanaka, G., Yamane, T., Héroux, J. B., Nakane, R., Kanazawa, N., Takeda, S., Numata, H., Nakano, D., & Hirose, A. (2019). Recent advances in physical reservoir computing: A review. Neural Networks, 115, 100–123. https://doi.org/10.1016/j.neunet.2019.03.005

Virtanen, P., Gommers, R., Oliphant, T. E., et al. (2020). SciPy 1.0: Fundamental algorithms for scientific computing in Python. Nature Methods, 17, 261–272. https://doi.org/10.1038/s41592-019-0686-2

Wang, G., Jiang, S., Wang, X., Shen, Y., & Yuan, F. (2016a). A novel memcapacitor model and its application for generating chaos. Mathematical Problems in Engineering, 2016, Article 3173696. https://doi.org/10.1155/2016/3173696

Wang, G., Zang, S., Wang, X., Yuan, F., & Iu, H. H.-C. (2017). Memcapacitor model and its application in chaotic oscillator with memristor. Chaos, 27(1), Article 013110. https://doi.org/10.1063/1.4973238

Wang, G.-Y., Cai, B.-Z., Jin, P.-P., & Hu, T.-L. (2016b). Memcapacitor model and its application in a chaotic oscillator. Chinese Physics B, 25(1), Article 010503. https://doi.org/10.1088/1674-1056/25/1/010503

Yuan, F., Li, Y., Wang, G., Dou, G., & Chen, G. (2019). Complex dynamics in a memcapacitor-based circuit. Entropy, 21(2), Article 188. https://doi.org/10.3390/e21020188

Yuan, F., Wang, G., Shen, Y., & Wang, X. (2016). Coexisting attractors in a memcapacitor-based chaotic oscillator. Nonlinear Dynamics, 86, 37–50. https://doi.org/10.1007/s11071-016-2870-6